




Research Article

Dynamic analysis of shallow embedded jacket offshore structures under wave forces

Yanzhao Yuan¹  · Xiancheng Wang¹

Received: 19 June 2022 / Accepted: 17 October 2022

Published online: 29 October 2022

© The Author(s) 2022 

Abstract

In this paper, the stress of temporary structures during the construction of offshore structures is analysed through the study of the temporary buried drilling platform. Firstly, The fluid flow is controlled by the modified RANS equation (the Reynolds-average equation) and Forchheimer saturation resistance model, the free surface is tracked by volume of fluid (VOF) method, and the κ - ϵ closed equation is solved. The finite element numerical simulation software is used to establish a multi-factor coupling calculation model of the stress of temporary buried offshore structures. The maximum wave force of temporary structures under different buried depths, different structural sizes, different load periods and amplitudes is simulated, and the stability of Long Yuan wind turbine pile foundation drilling platform under the maximum wave force is analyzed. The research results of this paper can be used for dynamic design and analysis of wave load conditions, structural design dimensions and load periods in the engineering design of embedded offshore structures in shallow water under wave loads, so as to calculate the wave load values of structures reasonably and provide concrete theoretical basis for the establishment of offshore systems.

Keywords RANS equation · Shallow-buried offshore structures · Max. wave load

1 Introduction

With the vigorous development of the transportation and marine engineering, many temporary buried structures (wind-driven pile drilling platforms, oil drilling platforms, etc.) have been built in offshore areas. Compared with long-term buried offshore structures (wind turbine pile foundation, bridge foundation of cross-sea bridge, etc.), the stability and safety of shallow buried structures are much lower than those of permanently buried structures because of their engineering characteristics. However, during the drilling process, the temporary buried structures needs to provide a stable platform for equipment [1, 2]. Therefore, the stress analysis of the temporary buried structures under the action of waves can effectively

provide theoretical support for the economic and safety design of temporary buried structures [3–5].

Previous studies mainly focused on the permanent buried structures at sea, while there was little research on pile foundation construction platforms under the action of waves [6, 7]. However, the impact of wave force on temporary buried structures is much greater than that of permanent facilities. Therefore, as an essential consideration in designing and constructing temporarily buried marine structures, wave force has become a focus of scholars' research. For the cylindrical pile foundation common in offshore engineering [8, 9]. The calculation method of wave force is selected according to the structural size (the ratio d/l of the diameter d of the cylinder to wavelength l). For small-scale structures with $D/L < 0.2$,

Supplementary Information The online version contains supplementary material available at <https://doi.org/10.1007/s42452-022-05207-5>.

✉ Yanzhao Yuan, yyz@hncj.edu.cn | ¹College of Civil and Traffic Engineering, Henan University of Urban Construction, Pingdingshan 467036, China.



SN Applied Sciences

(2022) 4:320

| <https://doi.org/10.1007/s42452-022-05207-5>

SN Applied Sciences
A SPRINGER NATURE journal

the Morrison equation, which is semi-empirical and semi-theoretical, can be used, and the influence of structure size on the flow field can be ignored. For large-scale structures with $D/L \geq 0.2$, the scattering effect of the system on incident waves and the free surface effect between the design and the fluid surface is apparent, so the wave force should be calculated by diffraction theory [10–12]. The boundary element model established by He and Geng [11] is used to numerically study the diffraction of three-dimensional objects with arbitrary shapes in regular waves. Using numerical simulation, Kang [13] studied the diffraction of a large diameter vertical cylinder under the action of periodic waves. Teng [14] introduced in detail the construction scheme design and construction lowering process of single-wall steel hanging box cofferdam in offshore engineering. When the above-mentioned scholars study the structural wave force by theoretical calculation, experimental research and numerical simulation, they all ignored the influence of pore flow on the structural wave force of high-porosity seabed [15–17]. Therefore, the numerical analysis of the impact of the seabed on wave force on the single pile and the results showed that the seabed attenuated wave propagation and increased wave force [13, 15, 18, 19]. However, the above research does not involve the influence of the dynamic process, structural form, the buried depth, wave parameters and other factors on structural wave force [20–22] (Fig. 1).

Due to the scale effect and high cost of practical methods, the applicable conditions of theoretical research methods are limited. With the rapid improvement of computer efficiency, numerical research methods have been used widely. Therefore, this paper refers to Chen [13] and others to control the fluid movement based on the modified RANS equation, describes the influence of waves on the seabed, and establishes a three-dimensional coupling analysis model of the interaction between shallow consolidated structures under wave action, further studies the attenuation effect of the seabed on waves, the change of the flow field around the system, and the influence of wave parameters and the movement state of the structure on the wave force on the network, which provides a reference for the design and buried of the system.

2 The numerical model

In this paper, FIAC-3 D simulation software is used for modeling and analysis of the project. The simulation software is a program for three-dimensional explicit calculation based on finite difference method [23]. The model is designed by square network elements. The upper water layer is 20 m high, and the unit size is 0.5 m × 0.5 m. Figure 2 is a three-dimensional figure for numerical analysis of the stress model of shallow embedded offshore structures under wave action based on the drilling platform of a wind turbine pile foundation in Long Yuan. For



Fig. 1 The large diameter offshore drilling platform

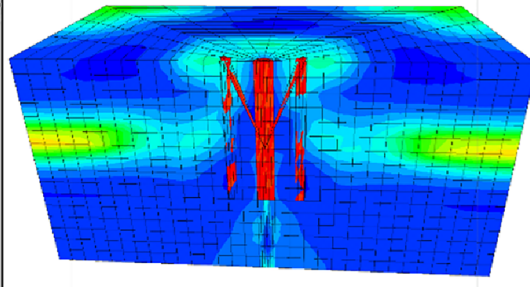
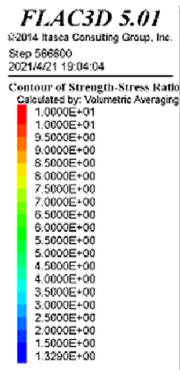
six platforms with a weight of over 550 t and a span of 23 m, the drilling liners extend to the relatively hard rock seabed with a depth of 1.5 m. Starting from the velocity boundary on the left side, the wave enters the propagation zone with sufficient length along the positive direction of the x -axis. x , y and z represent Cartesian coordinates; d_w stands for water depth; d_s represents the thickness of the seabed; H_0 represents the initial wave height; L stands for wavelength; D indicates the diameter of a single drilling liner; e means the relative buried depth, that is, the ratio of the structural depth d_m extending into the rocky seabed to the seabed thickness; The length, width and height of the computational domain along the coordinate axis are L_x , L_y and L_z , so it is necessary to calculate the value of the computational field in advance to minimise the influence of boundary conditions on the numerical analysis results. According to the test results, the calculation domain satisfies the following requirements: $L_x = 10 L$, $L_y = 100 D$, $L_z = 25$ m. In the subsequent numerical analysis, the ratio of structure width to numerical flume width is always less than 0.2, so the influence of flume width on the calculation results can be ignored. Unless otherwise stated, the analysis parameters are shown in Table 1.

2.1 The governing equations

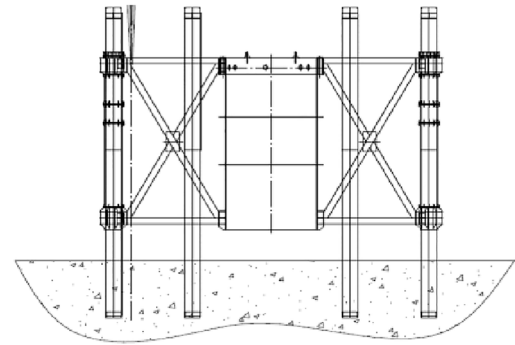
2.1.1 The fluid motion control

In this paper, according to RANS equation [24], the fluid load caused by waves is controlled, and the convergence of the equation is analyzed by using k - ϵ equation. The analysis formula is as follows.

$$\frac{\partial \langle u_i \rangle}{\partial x_i} = 0 \quad (1)$$



(a) Numerical simulation of strata



(b) Title system of six-legged pile platform

Fig. 2 Schematic diagram of numerical calculation of long-span particles on the rocky seabed

$$\frac{\partial \rho \langle u_i \rangle}{\partial t} + \frac{\partial \rho \langle u_i \rangle \langle u_j \rangle}{\partial x_j} = -\frac{\partial \langle p \rangle}{\partial x_i} + \frac{\partial}{\partial x_j} \left[\mu \left(\frac{\partial \langle u_i \rangle}{\partial x_j} + \frac{\partial \langle u_j \rangle}{\partial x_i} \right) \right] + \frac{\partial}{\partial x_j} \left(-\rho \langle u'_i u'_j \rangle \right) + \rho g_i - F_d u_i \tag{2}$$

where x_i is Cartesian coordinate; $\langle u_i \rangle$ is the overall average velocity component; this time ρ is fluid density; $\langle p \rangle$ is fluid pressure; μ is dynamic viscosity; g_i is the acceleration of gravity; $-F_d u_i$ is the resistance action term of porous media to water flow, that is, drag force. $-\rho \langle u'_i u'_j \rangle$ is Reynolds stress term, and $k-\epsilon$ turbulence equation can be used to simulate turbulent flow at high Reynolds number.

Boussinesq [7] put forward the calculation of eddy viscosity hypothesis of water flow, so Reynolds stress term can be expressed as:

$$-\rho \langle u'_i u'_j \rangle = \mu_t \left(\frac{\partial \langle u_i \rangle}{\partial x_j} + \frac{\partial \langle u_j \rangle}{\partial x_i} \right) - \frac{2}{3} \rho \delta_{ij} \kappa \tag{3}$$

where μ_t is turbulent viscosity; κ is turbulence kinetic energy; δ_{ij} is the Kronecker symbol.

Substituting formula (3) into formula (2), we can get

$$\frac{\partial \rho \langle u_i \rangle}{\partial t} + \frac{\partial \rho \langle u_i u_j \rangle}{\partial x_j} = -\frac{\partial}{\partial x_i} \left[\langle p \rangle + \frac{2}{3} \rho \kappa \right] + \frac{\partial}{\partial x_j} \left[\mu_{\text{eff}} \left(\frac{\partial \langle u_i \rangle}{\partial x_j} + \frac{\partial \langle u_j \rangle}{\partial x_i} \right) \right] \tag{4}$$

where $\mu_{\text{eff}} = \mu + \mu_t$ is the total effective viscosity.

In numerical analysis, the standard equation of $k-\epsilon$ turbulence is:

$$\frac{\partial \rho \kappa}{\partial t} + \frac{\partial \rho \langle u_j \rangle \kappa}{\partial x_j} = \frac{\partial}{\partial x_j} \left[\left(\mu + \frac{\mu_t}{\sigma_\kappa} \right) \frac{\partial \kappa}{\partial x_j} \right] + \rho P_\kappa - \rho \epsilon \tag{5}$$

$$\frac{\partial \rho \epsilon}{\partial t} + \frac{\partial \rho \langle u_j \rangle \epsilon}{\partial x_j} = \frac{\partial}{\partial x_j} \left[\left(\mu + \frac{\mu_t}{\sigma_\epsilon} \right) \frac{\partial \epsilon}{\partial x_j} \right] + \frac{\epsilon}{\kappa} (C_{\epsilon 1} \rho P_\kappa - C_{\epsilon 2} \rho \epsilon) \tag{6}$$

$$\mu_t = \rho C_\mu \frac{\kappa^2}{\epsilon} \tag{7}$$

$$P_\kappa = \frac{\mu_t}{\rho} \left(\frac{\partial \langle u_i \rangle}{\partial x_j} + \frac{\partial \langle u_j \rangle}{\partial x_i} \right) \frac{\partial \langle u_i \rangle}{\partial x_j} \tag{8}$$

where κ is turbulence kinetic energy; ϵ is the dissipation rate of turbulence kinetic energy; Parameters $C_\mu, \delta_\kappa, \delta_\epsilon, C_{\epsilon 1}$ and $C_{\epsilon 2}$ satisfy [23–25]: $C_\mu = 0.09, \delta_\kappa = 1.00, \delta_\epsilon = 1.30, C_{\epsilon 1} = 1.44$ and $C_{\epsilon 2} = 1.92$.

2.1.2 The movement control of drilling liner

Because of the rigidity of drilling liners, the movement of the drilling liners is usually regarded as a rigid body. According to the principle of kinematics, the movement of rigid body can be divided into translation and rotation. so the velocity V_p at a particular position of the rigid body is related to the velocity V_G and angular velocity of rigid body ω , which meets the following requirements [8].

$$V_p = V_G + \omega \times \gamma_{PG} \tag{9}$$

where γ_{PG} is the distance vector from $G \sim P$ of the centroid.

Table 1 Numerical analysis parameters

	Numerical value
Sea wave parameters	
Wave height H_0/m	5.0
Water depth d_w/m	20.0
Period T/s	6.0
Seabed parameters	
Seabed thickness d_s/m	15.0
Porosity n	0.4
Roughness factor β	0.04
Parameters of single pile	
Diameter of single pile D/m	8.0
Length of pile Lm/m	10.0
Relative buried depth e	2.0

2.1.3 Interaction between shallow drilling liners and seabed strata under wave action

Under the action of waves, the drilling liner will move horizontally and vertically, and the wave pressure will further change the water pressure of the soil. The height of the liner is h , and the depth of the seabed is d . The circulating force along the x -direction under the action of waves makes the bottom of the wellbore move along the z -direction and x -direction in the buried stratum. According to Biot’s consolidation theory [25], The effective stress variation of two-dimensional seabed soil satisfies the following equilibrium equation.

$$\frac{\partial \sigma_x}{\partial x} + \frac{\partial \tau}{\partial z} = \frac{\partial p}{\partial x} \tag{10}$$

$$\frac{\partial \sigma_x}{\partial z} + \frac{\partial \tau}{\partial x} = \frac{\partial p}{\partial z} \tag{11}$$

where σ_x/Pa and σ_z/Pa are effective stresses of soil in horizontal and vertical directions; τ/Pa is shear stress; p is excess pore water pressure.

The soil skeleton is regarded as an ideal isotropic elastic medium, and the constitutive equation of the seabed unit soil is.

$$\sigma_x = 2G \left[\frac{\partial u}{\partial x} + \frac{\mu}{1 - 2\mu} \epsilon_v \right] \tag{12}$$

$$\sigma_x = 2G \left[\frac{\partial w}{\partial z} + \frac{\mu}{1 - 2\mu} \epsilon_y \right] \tag{13}$$

$$\tau_{xx} = 2G \left[\frac{\partial u}{\partial z} + \frac{\partial w}{\partial N} \right] = \tau_{zx} \tag{14}$$

where G/Pa is the shear modulus of soil; μ is poisson’s ratio; τ_{zx}/Pa is the shear stress perpendicular to the xx -axis and along the z direction; τ_{zx} is the shear stress perpendicular to the z axis and along the x direction. Substituting formulas (9) to (11) into formulas (7) and (8) can be obtained:

$$G \nabla^2 u + \frac{G}{1 - 2\mu} \frac{\partial \epsilon_v}{\partial x} = \frac{\partial p}{\partial x} \tag{15}$$

$$G \nabla^2 w + \frac{G}{1 - 2\mu} \frac{\partial \epsilon_v}{\partial z} = \frac{\partial p}{\partial z} \tag{16}$$

2.2 The boundary conditions

According to the method proposed by Dean [26] to evaluate the applicable range of wave conditions, a fifth-order Stokes wave boundary is applied at the entrance boundary (X_{min}). The exit boundary (X_{max}) [27] adopts the Sommerfeld radiation boundary. When the edges of the numerical flume (Y_{min} and Y_{max}) assume a symmetric limit, waves can slide freely along the edges of the flume without penetrating. The wall boundary is adopted at the bottom and the structural surface of the numerical water tank (Z_{min}) to ensure that the average velocity of the fluid is zero and can not penetrate. At the top of the calculation field (Z_{max}), the pressure boundary is used, and the initial height of the fluid is specified. The VOF method locates and tracks the change of the free liquid surface [28]. The liquid volume function satisfies.

$$\frac{\partial F}{\partial t} + \frac{\partial (u_i F)}{\partial x_i} = 0 \tag{17}$$

The fluid volume function f represents the ratio of the fluid volume in the cell to the total fluid volume that can be accommodated. When $F = 0$, it means that the grid is full of gas, when $F = 1$, it means that the grid is full of fluid, and when $0 < F < 1$, it means that there are both gas and liquid in the grid, and it contains free water. Referring to the actual engineering construction process [8], In this paper, only the vertical and uniform descending motion of the drilling liner is considered. That is, the translation speed of the specified structure, and the remaining five degrees of freedom are all 0. In addition, the semi-coupling between structural motion and fluid means that the influence of structural motion on the flow field should be considered. However, the influence of the flow field on the structure signal has not been felt.

As shown in Fig. 2, the red marked pipe body of offshore single pile foundation is a large diameter steel pipe foundation. For this type of structural system, the pile-soil interaction system can be simplified as shown in Fig. 2. In Fig. 2, the dotted line indicates the pile, and the seabed soil in the lower light-coloured area can be described by the partial differential equations composed of Eqs. (4), (12) and (13), and the appropriate boundary conditions are established. The solution of pile-soil interaction in the ocean environment can be obtained by solving the partial differential equations. The seabed surface meets the following boundary conditions.

$$z = 0, \begin{cases} \sigma_x = 0 \\ \tau_{xx} = 0 \\ p = P_z \end{cases} \quad (18)$$

P_z is the wave pressure on the seabed, which is determined by the formula (3). The wave pressure on the seabed surface is determined by the formula (3).

$$z = -d, \begin{cases} u = 0 \\ w = 0 \\ \frac{\partial p}{\partial z} = 0 \end{cases} \quad (19)$$

And the interface between the liner and the seabed is impermeable to water. Assuming that the soil is not separated from the pile, the lateral displacement profile of the pile is linear. Under the action of linear waves, the time course of seabed soil displacement changes in sinusoidal curve, so does the time course of pile displacement. The left contact surface of pile-soil satisfies the following boundary conditions.

$$\begin{cases} u = y_0 \cdot (1 + z/l) \cos(kx - \omega t) \\ \frac{\partial p}{\partial x} = 0 \end{cases} \quad (20)$$

where y_0/m is the pile displacement at the mud surface; According to the equal transverse displacement on both sides of the pile, The boundary conditions of the pile-soil interface can be obtained.

$$\begin{cases} u = y_0 \cdot (1 + z/l) \cos(kx - \omega t - kb) \\ \frac{\partial p}{\partial x} = 0 \end{cases} \quad (21)$$

where $b(m)$ is the calculated width of the pile.

The left and right interfaces of seabed soil satisfy the following boundary conditions:

$$\begin{cases} \sigma_x = \sigma_0 \\ \frac{\partial p}{\partial x} = 0 \end{cases} \quad (22)$$

where σ_0/Pa is the confining pressure of soil. In the marine environment, the interaction system between the drilling casing and the earth can be expressed by the boundary conditions of partial differential equations composed of Eqs. (18), (19) and (20).

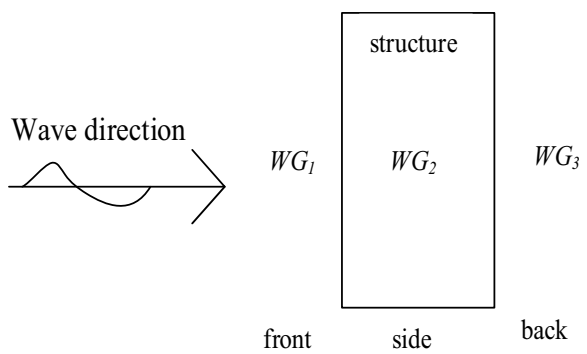
3 The model validation

In order to verify the accuracy of the model of the shallow-buried beam under wave action, and further study the stability of shallow-buried beam under different wave loads, the wave intensity around the interaction between wave and shallow-buried shaft and the stress of shallow-buried pile on rock seabed under wave action are analyzed.

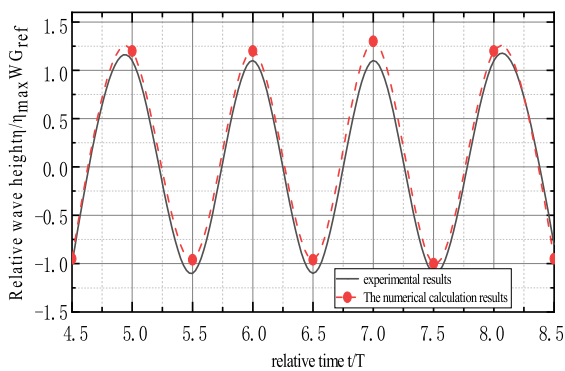
3.1 Environmental wave intensity under the interaction of waves and shallow buried shaft

Mo et al. [8]. designed a series of flume tests to study wave and single pile interaction. The water tank is 309 m in length, 5 m in width and 7 m in depth. The single pile is fixed at the bottom of the horizontal flume at a distance of 111 m from the wave generator. A plurality of wavemeters (WG) is arranged at different positions around the structure. The data of three typical locations (as shown in the Fig. 3) around the structure were compared: front (WG_1), side (WG_2) and back (WG_3). The wave parameters are water depth $d_w = 4.76$ m, wave period $T = 4$ s, wave height $H_0 = 1.2$ m, and single pile diameter $D = 0.7$ m.

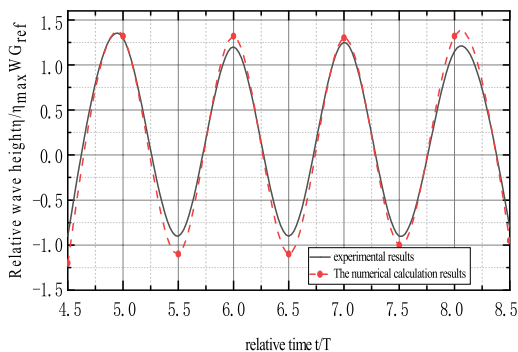
Figure 3 shows the time history curve of relative wave height. The wave height η is dimensionless by using η_{max} and WG_{ref} of the experimental data of the reference wave gauge (WG_{ref}). Because the reference wave gauge (WG_{ref}) is far away from the structure, the influence of the form on the wavefront can be ignored. The graphic results show that the measured data are consistent with the numerical results, and some characteristic ripples are well simulated. For example, when the wave trough passes through the drilling casing, the experimental and numerical results of the wave height at the front end (WG_1) show noticeable ripples. The results show that the numerical model can reasonably simulate the wave flow around the lining and provide reliable analysis results for the follow-up study of the wave forces on the structures under the wave action.



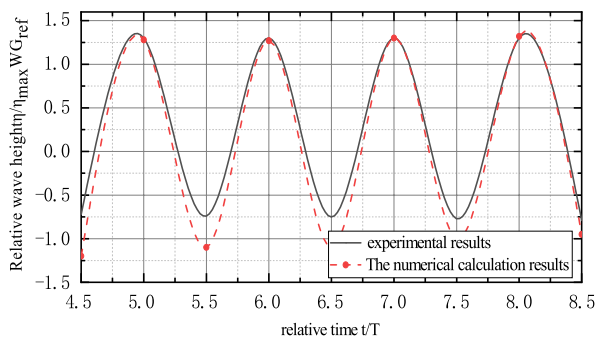
(a) Flume test diagram



(b) Front-end (WG_1) data comparison



(c) Side (WG_2) data comparison



(d) Backend (WG_3) data comparison

Fig. 3 Comparison of relative wave elevation time-history curves

3.2 The force of shallow embedded shaft on the rocky seabed under wave action

To consider the influence of rock seabed characteristics on wave forces on structures, a three-dimensional coupling model of wave-seabed-structure interaction is established, in which the rigidity ($n=0$) and elasticity ($n=0.5$) of the seabed are considered, respectively. To verify the accuracy of wave force calculation and the necessity of considering seabed characteristics, the numerical results of wave force F_x along the wave propagation direction of liners under different seabed conditions are compared with MacCamy's theoretical results. Figure 4 shows F_x time history curves under other seabed conditions. The comparison results show that the rigid seabed numerical analysis results agree with the MacCamy theoretical developments at the peak position. Still, there is a slight deviation at the valley position. This is mainly because the MacCamy theoretical formula does not consider the lateral force caused by vortex discharge behind the structure, which makes the amplitude of MacCamy's hypothetical results at the valley position more significant than the numerical analysis results of the rigid seabed. In addition, the maximum value of F_x in the elastic seabed is about 35% higher than that in the rigid seabed. It shows that the three-dimensional coupling model can accurately calculate the change of wave force on the structure under the condition of a rigid seabed, and the influence of seabed characteristics on the numerical value of wave force can not be ignored.

The numerical results show that the rock seabed can cause the attenuation of wave energy, but this does not mean that the wave force on the structure must definitely decrease. The wave forces in the designs will be affected by the wave conditions and the characteristics of rock seabed. Compared with rigid seabed, the rock characteristics of seabed will significantly affect the maximum F_x . Simplifying the rock seabed into frozen impermeable solid and ignoring the rock characteristics of the seabed will underestimate the force of waves on the structure. Therefore, it is necessary to comprehensively consider the influence of wave parameters on seabed and structural characteristics, and deeply analyze the forces exerted by wave on structures.

4 Discussion

4.1 The influence of wave parameters

The stress of shallow-buried shaft under wave action is mainly affected by local geological and hydrological conditions, so without considering the influence of the seabed, the wave parameters are more critical to the horizontal wave force of liners [7, 10, 29], and the

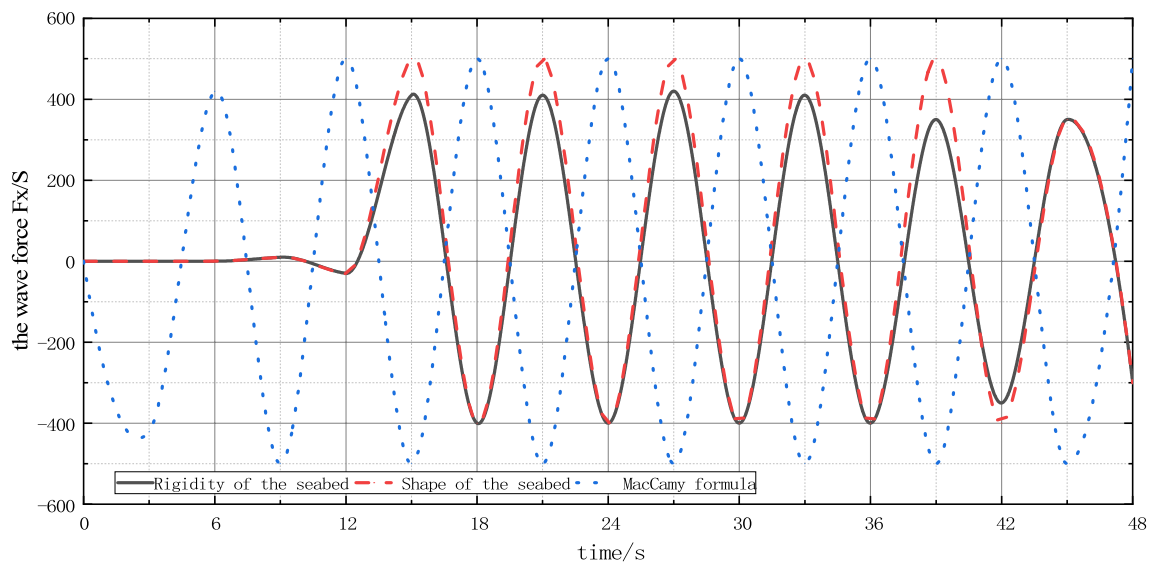


Fig. 4 Time history curve of wave force F_X on a single pile

calculation method of horizontal wave force of various structures under wave action is introduced in detail in "Hydrographic Code for Ports and Waterways (JTS 145-2015) [30]. Because researchers pay more attention to the attenuation of waves on the rocky seabed, there is little research on wave forces on structures extending to the elastic seabed. Therefore, the correlation between incident wave conditions and wave forces acting on the cushion layer is studied and compared with strict seabed conditions. the effects of period T , wave steepness (H_0/L) and relative water depth (d_w/L) on wave forces on the cushion were studied.

Figures 5, 6 and 7 show F_{Xmax} curves under different wave periods T , wave steepness (H_0/L) and relative water depth (d_w/L). The results show that the F_{Xmax} value increases linearly with the increase of wave parameters, but the increased range is different; The maximum value of wave force F_{Xmax} is sensitive to wave height and water depth. This means that the liners extending into the elastic seabed are subjected to greater wave forces under the action of big waves and long periods. This is because the wave energy is significant, and the projection area of the transverse structure to the wave propagation direction is substantial; that is, the reference volume is large, which makes the force borne by the cushion large. In addition,

Fig. 5 Under different period T conditions F_{Xmax} change curve

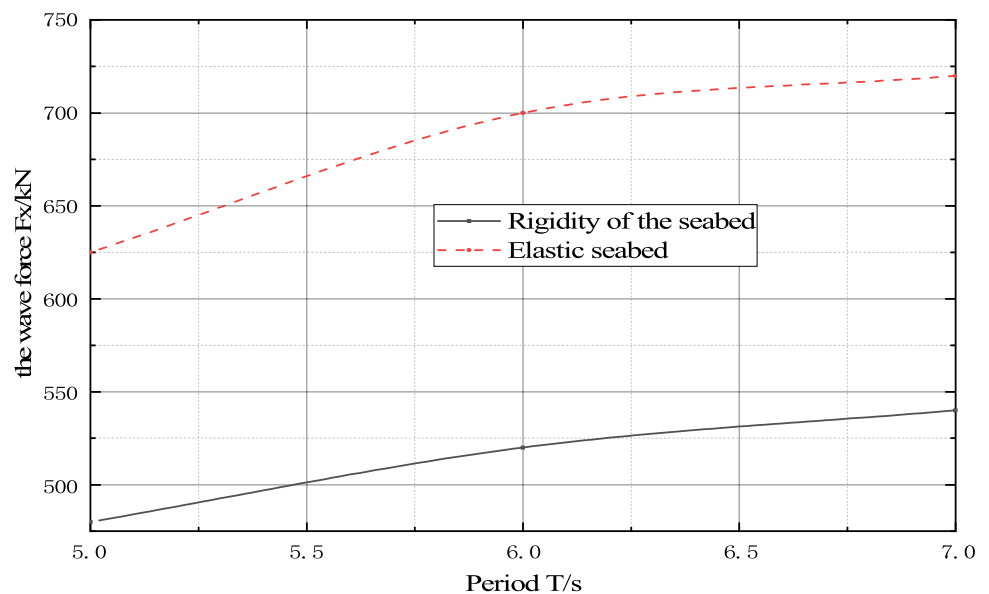


Fig. 6 Under different wave steepness (H_0/L) F_{xmax} change curve

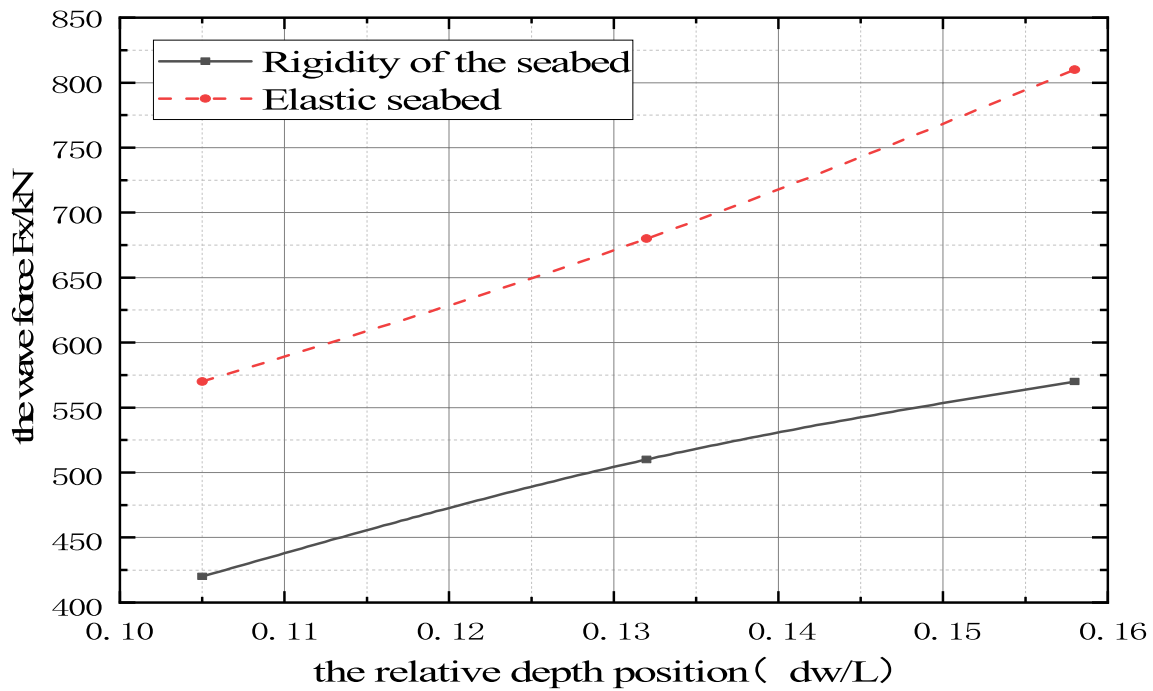
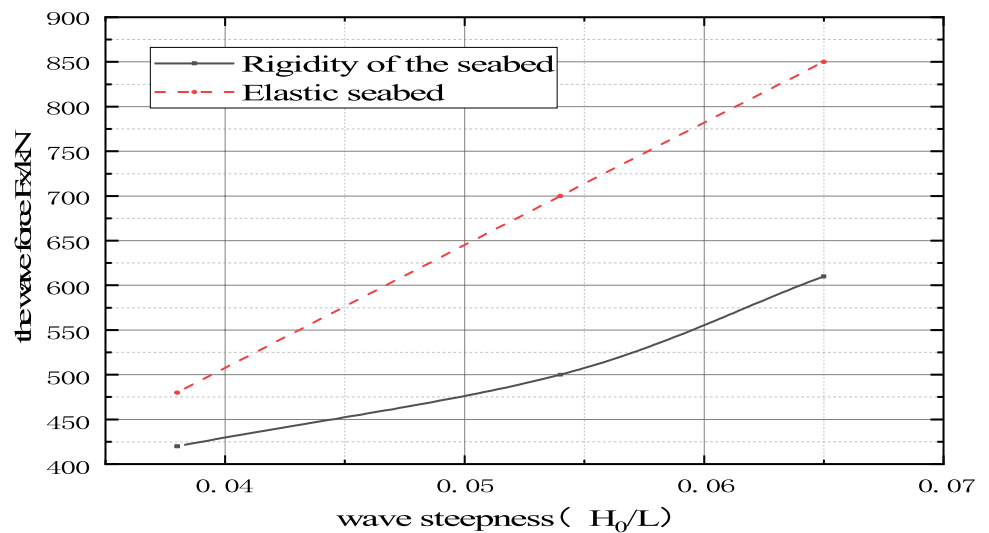


Fig. 7 F_{xmax} variation curves under different relative water depths (dw/L)

the value of elastic seabed F_{xmax} is greater than that of the rigid seabed. By comparing the analysis results, the importance of considering the seabed's strength in shallow-buried ocean engineering design is emphasised again.

4.2 The influence of structure characteristics

In engineering practice, the pile foundation's size will affect the structure's stress. In addition, during the initial structural design, various cross-section types, such as round, square or round end, will be compared, and

the embedding depth will be set. At the same time, the pile foundation structure is lowered during construction. Therefore, it is beneficial for structural safety to study the influence of cross-section diameter d , shape, buried depth (e) and construction lowering speed (v) on the dynamic response of structures.

4.2.1 The influence of structure diameter D

To study the influence of single pile diameter on wave force on a single pile considering the porous characteristics of

the seabed, the single pile diameter increased from 4 to 8 m under the same wave and seabed characteristics. Figure 8 is a time history curve of wave force F_x on a single pile. As shown in the figure, with the wave propagation, the value of wave force F_x oscillates with the wave period t , and the amplitude is stable when the wave is stable. In addition, the larger the diameter of a single pile, the larger the amplitude of wave force F_x on a single pile. This is because under the action of waves, the larger the diameter of a single pile, the larger the lateral stress area of the structure. In engineering practice, the diameter of systems can be determined concerning the traditional calculation method under the condition of high permeability seabed.

4.2.2 The influence of buried depth s of structures

According to the above analysis, the dynamic characteristics of the structure are influenced by the characteristics of elastic seabed, mainly due to the seepage inside the seabed. Then, the depth of the shallow-buried structures extends into the seabed is relatively shallow, so the elastic seabed has different influences on the stress of the shallow-buried structures according to the buried depth of liners. Figure 9 is the variation curve of F_x and $F_{x_{max}}$ under the condition of relative burial depth of different structures. The results show that, with the increase of buried depth S , the change period of F_x is the same, and $F_{x_{max}}$ increases linearly with the increase of buried depth. This is because the stress calculation length of shallow buried structures increases linearly. The calculated stress length of a single pile with $s = 1$ is always more meaningful than that of a single pile with $s = 0$, and the seabed thickness is d_s . In engineering practice, for the elastic seabed, the influence of seabed characteristics and the influence of lining

buried depth on structural stress should be considered in the consolidation design.

4.3 The displacement analysis of structures in soil layer

According to the functional condition design of the offshore drilling platform of Long Yuan Group, the specific parameters are shown in Table 1. According to the model analysis, $F_x = 610$ KN, calculated area: $-400 \text{ m} \leq x \leq 400$; $-100 \text{ mm} \leq z \leq 0$. Figure 5 shows the wave pressure of a boring steel cofferdam under different deflections. It can be seen from the figure that when the deflection of the steel cofferdam exceeds 10 mm and the soil conditions are unchanged, the earth pressure on the pile will decrease, which is consistent with the description in the code for pile foundation. Figure 10a and b shows the effective normal stress distribution of the soil around the steel cofferdam under different deflections. It can be seen from these figures that the deflection of the steel cofferdam has little effect on the normal stress of the underlying soil. Figure 10c and d represents the relative horizontal and vertical displacement distribution of soil in the free field. It can be seen from the figure that the horizontal and vertical displacement of the seabed soil gradually decrease along the depth direction, and become zero at a certain depth. The vertical displacement attenuates rapidly, and the influence of horizontal displacement on the bearing capacity of steel cofferdam can not be ignored. Based on the horizontal displacement distribution diagram and Wink foundation beam model, the response of the offshore pile foundation can be calculated accurately.

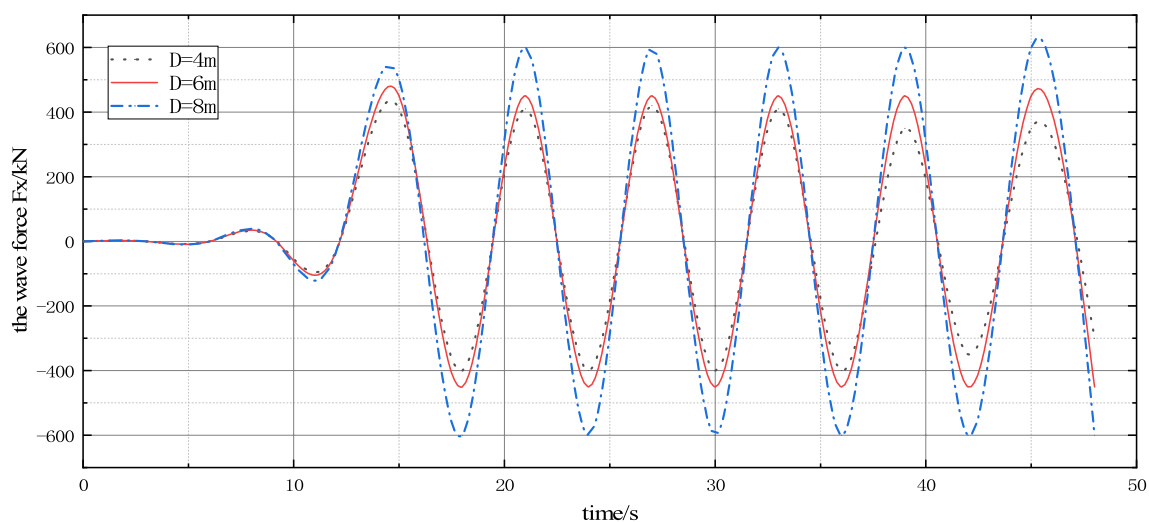
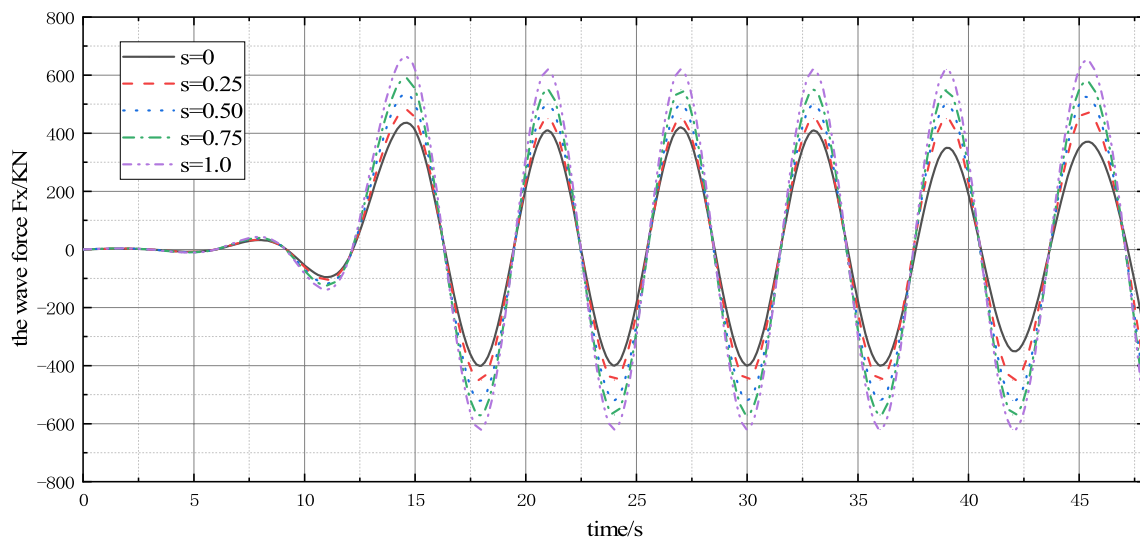
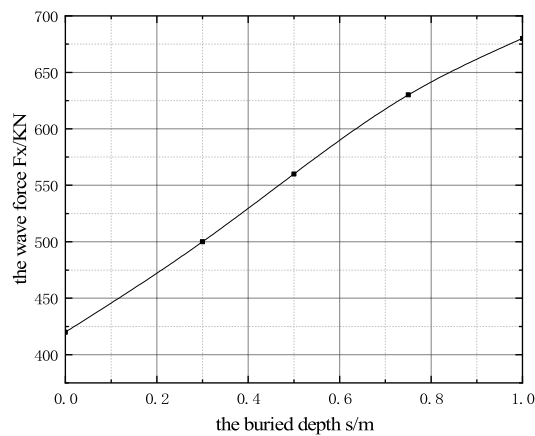


Fig. 8 The time history curve of F_x under different pile foundation diameter D



(a) F_x change curve under different burial depths



(b) $F_{x_{max}}$ variation curves under different buried depths

Fig. 9 F_x and $F_{x_{max}}$ variation curves under different buried depth s

5 Conclusion

The finite element numerical simulation method is used to analyze the wave forces of offshore shallow buried structures under various working conditions. The effects of the rigid and elastic seabed on buried structures, buried depth and structures, and structural characteristics on structural forces are studied, as well as the stability of shallow buried systems under different wave forces. The following conclusions and suggestions are obtained: three-dimensional coupled numerical model of waves on buried offshore structures in shallow water can better reflect the attenuation effect of waves, and can be further used to study the forces of waves on structures. During the process of design and construction of drilling

pipe, the influence of seabed elasticity on structural wave forces should not be ignored. Due to the influence of wave energy and the volume of the structure, the structure extends into the deep-water elastic seabed. Under the action of big waves, high waves and long periods, the system is subjected to relatively large wave force. In structural design and construction, it is necessary to choose reasonable wave parameters.

Under the same wave conditions, the larger the diameter of the structure is, the larger the amplitude of F_x is. Due to the influence of reference volume and surface curvature, the cross-sectional shape of the system will affect the stress of the structure. $F_{x_{max}}$ increases linearly with the increase of buried depth, and F_x increases periodically in the process of lowering the structure at a uniform speed.

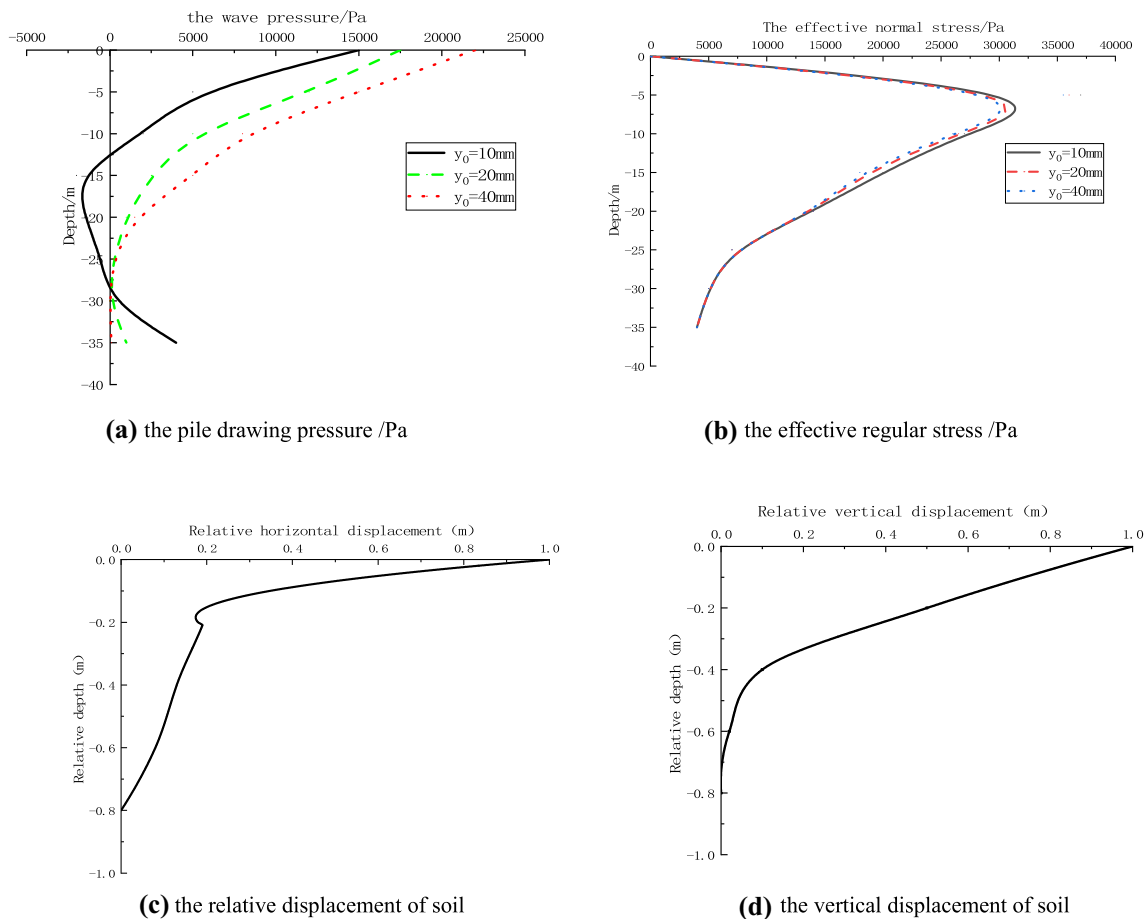


Fig. 10 The analysis of calculation results

The amplitude of F_x is stable when the system is at rest on the seabed surface. The faster the descent speed, the faster the wave reaches stability, but the amplitude is the same. The numerical examples show that, under the action of waves, the horizontal displacement and vertical displacement of seabed soil gradually decrease along the depth direction, and the vertical displacement decreases rapidly. The influence of horizontal displacement on the bearing capacity of offshore pile foundations can not be ignored. The response of "passive pile" in the marine environment can be accurately calculated by combining the plane displacement distribution diagram obtained from the analysis of the Wink foundation beam model.

Through the related calculation and numerical analysis in this paper, the stability of shallow-buried offshore drilling platform under the geological conditions of rock seabed in South China Sea is analyzed and discussed. Therefore, it is necessary to calculate the stability of shallow water drilling platforms under different seabed conditions in the later research.

Acknowledgements We thank Henan Disaster Prevention and Mitigation Engineering Center for providing equipment support for this experiment.

Author contributions YY: Conceptualization, YY, XW: data curation, XW: formal analysis, YY: methodology, XW: resources, YY: visualization, YY: writing—original draft, YY: writing—review and editing.

Funding The author Y. Yuan study was supported by National Natural Science Foundation of China (Grant No. 52004081) and X. Wang study also supported by Public Relations Program of Science and Technology of Henan Province (Industrial Field) Project (Grant No. 182102210221).

Data availability All relevant data are within the paper and its Supporting Information files.

Declarations

Conflict of interest The authors have no competing interests to declare that are relevant to the content of this article.

Open Access This article is licensed under a Creative Commons Attribution 4.0 International License, which permits use, sharing, adaptation, distribution and reproduction in any medium or format, as long as you give appropriate credit to the original author(s) and the source, provide a link to the Creative Commons licence, and indicate if changes were made. The images or other third party material in this article are included in the article's Creative Commons licence, unless indicated otherwise in a credit line to the material. If material is not included in the article's Creative Commons licence and your intended use is not permitted by statutory regulation or exceeds the permitted use, you will need to obtain permission directly from the copyright holder. To view a copy of this licence, visit <http://creativecommons.org/licenses/by/4.0/>.

References

1. Duan L, Liao C, Jeng D, Chen L (2017) 2D numerical study of wave and current-induced oscillatory non-cohesive soil liquefaction around a partially buried pipeline in a trench. *Ocean Eng* 135:39–51. <https://doi.org/10.1016/j.oceaneng.2017.02.036>
2. Chen L, Liao C, Duan L, Zheng D (2017) Numerical analysis of wave-porous media sea-pile interaction. In: Chinese mechanics conference—2017 and celebration of the 60th anniversary of the Chinese Society of Mechanics, Beijing, China, vol 13. <https://doi.org/10.1016/j.oceaneng.2018.02.041>
3. Qi W-G, Li Y-X, Kai Xu, Gao F-P (2019) Physical modelling of local scour at twin piles under combined waves and current. *Coast Eng* 143:63–75. <https://doi.org/10.1016/j.coastaleng.2018.10.009>
4. Zhen KA, Bing Z, Fan X, Xing H (2014) Numerical simulation of large structures subjected to wave forces. *J Eng Mech* 31:108–115. <https://doi.org/10.1016/j.jfluidstructs.2014.05.011>
5. Kantardgi I, Zheleznyak M, Demchenko R et al (1963) Modeling of nonlinear hydrodynamics of the coastal areas of the Black Sea by the chain of the proprietary and open source models. *Nauchni Tr Vissh Med Inst Sofia* 42(12):77–83. <https://doi.org/10.1016/j.oceaneng.2020.107673>
6. Jeng DS, Ye JH, Zhang JS, Liu LF (2013) An integrated model for the wave-induced seabed response around marine structures: model verifications and applications. *Coast Eng* 72:1–19. <https://doi.org/10.1016/j.coastaleng.2012.08.006>
7. Behera H, Mandal S, Sahoo T (2013) Oblique wave trapping by porous and flexible structures in a two-layer fluid. *Phys Fluids* 25:23–42. <https://doi.org/10.1063/1.4832375>
8. Mo W, Kai I, Oumeraci H, Liu LF (2007) A 3D numerical model for computing non-breaking wave forces on slender piles. *J Eng Math* 58:19–30. <https://doi.org/10.1007/s10665-006-9094-6>
9. Karunarathna SA, Lin P (2006) Numerical simulation of wave damping over porous seabeds. *Coast Eng* 53:845–855. <https://doi.org/10.1016/j.coastaleng.2006.05.003>
10. Jeng DS, Zhang H (2005) An integrated three-dimensional model of wave-induced pore pressure and effective stresses in a porous seabed: II. Breaking waves. *Ocean Eng* 32:1950–1967. <https://doi.org/10.1016/j.oceaneng.2005.01.005>
11. He W, Geng J (2005) Boundary element model for solving wave loads of three-dimensional objects. *Eng Mech*. <https://doi.org/10.1016/j.enganabound.2009.04.005>
12. Subrata KC (1994) *Offshore structure modeling*. World Scientific Publishing Company, Singapore. <https://doi.org/10.1142/2127>
13. Gong S, Pu X, Sheng B et al (2014) Numerical modelling on dynamic behaviour of deepwater S-lay pipeline. *Ocean Eng* 88:393–408. <https://doi.org/10.1016/j.oceaneng.2014.07.016>
14. Teng J. Construction technology of single wall steel box cofferdam for Pier No. 4 of Minjiang Bridge in Langqi. *World Bridge* 40, 37–40 (2012)
15. Trapper PA (2020) Static analysis of offshore pipe-lay on flat inelastic seabed. *Ocean Eng* 213:107673. <https://doi.org/10.1016/j.oceaneng.2020.107673>
16. Song K, Guo C, Gong J, Li P, Wang L (2018) Influence of interceptors, stern flaps, and their combinations on the hydrodynamic performance of a deep-vee ship. *Ocean Eng* 170:306–320. <https://doi.org/10.1016/j.oceaneng.2018.10.048>
17. Hammad A, Abdel-Nasser Y, Shama M (2021) Rational design of T-Girders via finite element method. *J Mar Sci Appl*. <https://doi.org/10.1007/s11804-021-00206-1>
18. Zhao TF, Zhang QY, Chu G (2021) Truss-type maintenance devices and corresponding pipeline lifting control strategies. *Pet Sci* 18:939–950. <https://doi.org/10.1007/s12182-021-00545-2>
19. Zhao Q, Guo C, Su Y et al (2017) Study on unsteady hydrodynamic performance of propeller in waves. *J Marine Sci Appl* 16:305–312. <https://doi.org/10.1007/s11804-017-1419-5>
20. Wang LZ, Guo CY, Su YM, Wu TC (2018) A numerical study on the correlation between the evolution of propeller trailing vortex wake and skew of propellers. *Int J Naval Architect Ocean Eng* 10(2):212–224. <https://doi.org/10.1016/j.ijnaoe.2017.07.001>
21. Wang L, Guo C, Su Y, Xu P, Wu T (2017) Numerical analysis of a propeller during heave motion in cavitating flow. *Appl Ocean Res* 66:131–145. <https://doi.org/10.1016/j.apor.2017.05.001>
22. Sun C, Guo C, Wang C, Wang L, Lin J (2020) Numerical and experimental study of flow field between the main hull and demi-hull of a trimaran. *J Mar Sci Eng* 8(12):975. <https://doi.org/10.1155/2014/917975>
23. Chen L, Zheng D, Wang P, Zhu B (2019) Wave force analysis of single pile foundation based on wave-porous media sea-structure coupling model. *Eng Mech* 36:81–91. <https://doi.org/10.29328/journal.acee.1001003>
24. Wang L, Guo C, Su Y, Wu T, Wang S (2017) Numerical study of the viscous flow field mechanism for a non-geosim model. *J Coast Res* 33(3):684–698. <https://doi.org/10.2112/JCOAS-TRES-D-16-00036.1>
25. Fenton JD (1985) A fifth-order Stokes theory for steady waves. *J Waterw Port Coast Ocean Eng* 111(2):216–234. [https://doi.org/10.1061/\(ASCE\)0733-950X\(1985\)111:2\(216\)](https://doi.org/10.1061/(ASCE)0733-950X(1985)111:2(216))
26. Biot A (1956) M: Theory of deformation of a porous viscoelastic anisotropic solid. *J Appl Phys* 27:459–467. <https://doi.org/10.1063/1.1722402>
27. Dean RG (1970) Relative validities of water wave theories. *J Waterw Harb Coast Eng Div* 97:212–213. https://doi.org/10.1007/978-1-84996-190-5_3
28. Savage RP, Fairchild JC (1953) Laboratory study of wave energy losses by bottom friction and percolation. *USACE Beach Erosion Board Tech* 5(4):234–237. [https://doi.org/10.1016/0141-1187\(83\)90038-X](https://doi.org/10.1016/0141-1187(83)90038-X)
29. Wang W, Yang M (2012) Key technical issues and discussion of offshore wind turbine infrastructure design. *J Hydroelectr Eng*. <https://doi.org/10.1016/j.rser.2007.07.004>
30. Code for Hydrology of ports and waterways (2015)

Publisher's Note Springer Nature remains neutral with regard to jurisdictional claims in published maps and institutional affiliations.